Editors' Suggestion | Featured in Physics

Quantum Optical Microphone in the Audio Band

Raphael Nold,[1,2] Charles Babin,[1,2] Joel Schmidt,[1,2] Tobias Linkewitz,[1,2] María T. Pérez Zaballos,[3] Rainer Stöhr,[1,2] Roman Kolesov,[1,2] Vadim Vorobyov,[1,2] Daniil M. Lukin,[4] Rüdiger Boppert,[5] Stefanie Barz,[2,6] Jelena Vučković,[4] J. Christof M. Gebhardt,[2,7] Florian Kaiser,[1,2,*] and Jörg Wrachtrup[1,2]

[1] *3rd Institute of Physics and Stuttgart Research Center of Photonic Engineering (SCoPE), University of Stuttgart, 70569 Stuttgart, Germany*

[2] *Center for Integrated Quantum Science and Technology (IQST), Germany*

[3] *The Old Schools, Trinity Lane, Cambridge CB2 1TN, United Kingdom*

[4] *Ginzton Laboratory, Stanford University, Stanford, California 94305, USA*

[5] *Department of Pediatric Audiology and Neurotology, Olgahospital, 70174 Stuttgart, Germany*

[6] *Institute for Functional Matter and Quantum Technologies, University of Stuttgart, 70569 Stuttgart, Germany*

[7] *Institute of Biophysics, Ulm University, 89081 Ulm, Germany*

(Received 24 January 2022; revised 26 April 2022; accepted 19 May 2022; published 17 June 2022)

The ability to perform high-precision optical measurements is paramount in science and engineering. Laser interferometry enables interaction-free sensing with a precision ultimately limited by shot noise. Quantum optical sensors can surpass this limit but single- or multiphoton schemes are challenged by low experimental sampling rates, while squeezed-light approaches require complex optical setups and sophisticated time gating. Here, we introduce a simple method that infers optical phase shifts through standard intensity measurements while still maintaining the quantum advantage in the measurement precision. Capitalizing on the robustness and high sampling rates of our device, we implement a quantum optical microphone in the audio band. Its performance is benchmarked against a classical laser microphone in a standardized medically approved speech-recognition test on 45 subjects. We find that quantum-recorded words improve the speech-recognition threshold by -0.57 dB_{SPL}, thus making the quantum advantage audible. Not only do these results open the door toward applications in quantum nonlinear interferometry but they also show that quantum phenomena can be experienced by humans.

DOI: 10.1103/PRXQuantum.3.020358

Optical interferometry represents the gold standard for measuring small displacements [1], refractive indices [2,3], and surface properties [4,5]. A textbook example is the Michelson interferometer. Here, the best achievable phase sensitivity, $\Delta\Phi$, with N uncorrelated photons is given by the shot-noise limit (SNL) [6–8], $\Delta\Phi = 1/\sqrt{N}$. Quantum optical sensors surpass the SNL by exploiting correlations and entanglement [7–13]. Theoretically, N-photon entangled quantum states can reach Heisenberg scaling, $\Delta\Phi = 1/N$, which is the ultimate sensitivity limit [6,8,9]. This can be understood by considering the N-photon entangled state as a single entity in which all photons accumulate a collective phase [14], $N\Delta\Phi$. Importantly, information about each N-photon quantum state is extracted in a single experimental repetition. This is different from the classical case based on N uncorrelated photons that acquire phase shifts individually, thus necessitating N single-photon measurements. The fact that the noise power of a measurement increases with the square root of the repetitions makes it clear that the quantum strategy can improve the signal-to-noise ratio (SNR) by a factor of $\sqrt{N}$.

Although quantum optical phase sensing has been implemented with multiphoton-path entangled states [2,15,16], the achievable low repetition rates hinder the development of applications. This is mainly a conceptual issue. Traditional schemes require measurement of whether an even or odd number of photons leaves each interferometer output port [17]. For $N = 2$, this imposes the use of single-photon detectors (SPD) to distinguish between zero and one photons, while experiments

*Corresponding author. f.kaiser@pi3.uni-stuttgart.de

with $N > 2$ necessitate photon-number-resolving detectors (PNRDs) [18,19]. The associated measurement rates tend to be slow, as these detectors show low optical saturation levels [20] and complex coincidence counting is involved [8].

The saturation problem can be overcome using standard photodetectors in pulsed squeezed-light experiments; however, due to the pulsed regime, the effective measurement duty cycle is typically very low, thus limiting overall sampling rates [21–23]. 100% duty cycle is obtained with continuous-wave squeezed light; however, it comes at the cost of complex setups [24,25] and instabilities at high pump powers [26–28]. In this field, the sensitivity of squeezed states of light to loss [29–32], which compromises the overall sensitivity, remains a challenge.

Recent approaches thus rely on nonlinear interferometry in SU(1,1) interferometer arrangements [11,33] but these schemes face challenges in addressing common-mode noise (pump-laser power fluctuations) [11,33,34].

Alternative measurement concepts have been inspired by fundamental quantum optics research in the 1990s, where the concept of "induced coherence without induced emission" was introduced as an elegant way to create photonic superposition states [35,36] that can reach superresolution [37]. This has subsequently led to the development of "quantum imaging with undetected photons" [38–40] and "two-photon phase sensing with single-photon detection" [41]. However, phase sensing beyond the classical limit has not been demonstrated.

Here, we build upon these creative ideas and combine them with path-polarization quantum state engineering [41] to show sub-shot-noise phase sensing, while pushing the sampling rates of previous experiments based on photon-number states [2,16] by 4 orders of magnitude. Capitalizing on these advances, we introduce a quantum optical microphone that surpasses the performance of an equivalent laser microphone. By benchmarking the microphone performance in a standardized audiology test on $n = 45$ individuals, we provide a human experience of a quantum phenomenon; in other words, we make the quantum advantage audible.

The underlying idea of our sensing concept considers the canonical multiphoton-path entangled state that acquires a phase: $|\Psi\rangle_{\text{path}} = (|N\rangle_a|0\rangle_b + e^{(iN\Delta\Phi)}|0\rangle_a|N\rangle_b)/\sqrt{2}$, where N is the photon number, while a and b denote the two different paths. This work focuses on the case $N = 2$, for which we will show that, via quantum state engineering, we can transfer the two-photon phase information deterministically to a single-photon polarization state: $|\Psi\rangle_{\text{path}} = (|\text{V}\rangle + e^{(iN\Delta\Phi)}|\text{H}\rangle)/\sqrt{2}$, where V and H denote vertical and horizontal polarization modes. At this point, the phase $N\Delta\Phi$ can be extracted from a simple intensity-difference measurement after a polarizing beam splitter, in one-to-one correspondence with classical interferometry based on single-photon interference. This has two critical implications. First, the basic intensity detection is sufficient such that no single photon or homodyne detection is required. Additionally, the difference-intensity detection scheme can be efficiently used to reject common-mode noise, thus providing improved robustness and reliability.

I. PHASE-MEASUREMENT SCHEME

The experimental setup is detailed in Fig. 1. A 532-nm continuous-wave pump laser (green lines) is sent forward through a periodically poled potassium titanyl phosphate nonlinear crystal (PPKTP) and is retroreflected at the reference mirror (RM) for a second backward passage. Via type-0 collinear parametric down-conversion in the PPKTP, each laser photon has a small chance of creating a nondegenerate signal-idler photon pair contribution in either direction, $|V,s\rangle_f|V,i\rangle_f$ or $|V,s\rangle_b|V,i\rangle_b$, respectively (red and orange lines). The subscripts f and b indicate photon-pair generation in the forward and backward direction, respectively, the wavelengths of which are 1109 nm (s, signal) and 1023 nm (i, idler). By adjusting the pump power, we generate a photon-pair flux of approximately

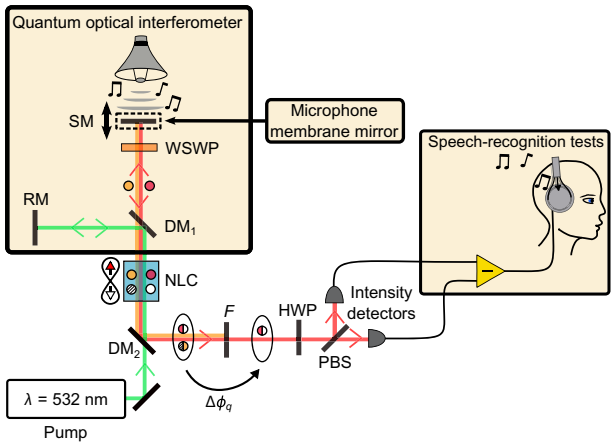

FIG. 1. The advanced quantum optical sensor. A 532-nm laser pumps a nonlinear crystal (NLC) to generate photon pair contributions in the forward and backward directions after reflection on the reference mirror (RM). The forward-generated pair contribution acquires the two-photon phase shift induced by displacements of the sample mirror (SM). The SM can be replaced by a microphone-membrane mirror to implement an acousto-optical transducer for recording human speech. After a double passage through the wavelength-selective wave plate (WSWP), the forward- and backward-generated pair contributions are overlapped without interference, which effectively transfers the two-photon phase shift onto a single-photon state. A filter (F) transmits only the relevant single-photon state, from which the two-photon phase shifts are reconstructed via simple light-intensity detection at sampling rates up to 100 kHz. The intensity-difference signal can be directly used to test the performance of the quantum microphone in a medical speech-recognition test on humans. DM, Dichroic mirror splitting up pump-laser light and photon pairs.

$1.65 \times 10^8 s^{-1}$, which undercuts the parametric threshold value ($7.02 \times 10^{12} s^{-1}$; see the Supplemental Material [42]) and thus we operate in the regime of individual photon pairs.

The forward-generated photon pair contribution is retroreflected at the sample mirror (SM). Depending on the experiment, the SM is either a bulk mirror or a mirror membrane that is sensitive to sound waves. The distance at which the SM is placed with respect to the RM defines the two-photon phase shift $\Delta\Phi_q = \Delta\Phi_s + \Delta\Phi_i$. Here, $\Delta\Phi_s$ and $\Delta\Phi_i$ are the individual phase shifts accumulated by the signal and idler photon, respectively. One critical feature in our scheme is the dual passage of the forward-generated pair contribution through a wavelength-selective wave plate (WSWP). The WSWP rotates, after a dual passage, the polarization of the signal photon by 90° while maintaining the idler-photon polarization; thus the quantum state is transformed to $e^{(i\Delta\Phi_q)}|\mathrm{H}, s\rangle_f |\mathrm{V}, i\rangle_f$. The advantage of the WSWP is that both photons in the forward-generated pair contribution accumulate the phase shift from the same path and are reflected at the same point on the sample mirror. Additionally, the creation of a cross-polarized state avoids interference when subsequently overlapping forward- and backward-generated pair contributions. After overlapping both pair contributions into the same spatial mode, their subscripts f and b become obsolete, such that we have

$$|\Psi\rangle_{\mathrm{path}} = \left(\frac{|\mathrm{V,s}\rangle + e^{(i\Delta\Phi_q)}|\mathrm{H,s}\rangle}{\sqrt{2}}\right)|\mathrm{V,i}\rangle. \tag{1}$$

As intended, we imprint the two-photon phase shift $\Delta\Phi_q$ onto the signal single-photon state. As the idler photon does not carry useful information, we reject it using a 1109 ± 2 nm band-pass filter. After the filter, phase information from the remaining signal photons is accessed via a projective measurement in the σ_x basis. Experimentally, this is implemented using a half-wave plate (HWP), a polarizing beam splitter (PBS), and two intensity detectors, $D_\pm$. The measured detector signals are as follows:

$$I_\pm \propto 1 \pm \nu_q \cos(\Delta\Phi_q), \tag{2}$$

in which the fringe visibility ν_q includes experimental imperfections, such as detector noise, loss, and nonoptimal spatial mode overlap (see the Supplemental Material [42]). The application-relevant key advantage of our scheme is that the two-photon phase $\Delta\Phi_q$ is now accessible with standard intensity measurements, including common-mode noise rejection. Consequently, classical and quantum sensors can be directly compared using the same detection schemes; for example, using detectors with high sampling rates.

II. BENCHMARKING THE QUANTUM ADVANTAGE

As our quantum phase sensor resembles a Michelson-type interferometer, we naturally compare it to a classical Michelson interferometer operated with laser light at the average wavelength of the photon pairs (1064 nm; for setup details, see the Supplemental Material [42]). For both schemes, we define as a resource the quantity of photons entering the interferometer; thus challenges associated with the quantum strategy (loss inside the interferometer and nonperfect mode overlap inside the NLC) are explicitly not corrected for. Further, to benchmark the sensing schemes at the purest and fundamental level, it is important to minimize parasitic noise from the intensity detectors. This is why we use superconducting-nanowire photon detectors (SNPDs) for this demonstration. However, we emphasize that the SNPDs are operated as low-noise intensity detectors and that their single-photon detection capability is not required.

In a first step, we induce controlled phase shifts in the classical and quantum interferometers by transducing the sample mirror with a piezoelectric actuator. The resulting difference intensities between the two output detectors are shown in Fig. 2(a). For the same piezo displacement, the quantum sensor displays twice as many interference fringes. This corroborates the use of path-entangled two-photon states that acquire phase information with superresolution. However, superresolution is not sufficient to demonstrate an exploitable quantum advantage [8]. The critical parameter to consider is the achievable phase sensitivity per photon sent to the interferometer.

For the classical sensing scheme (subscript c), the optimal phase sensitivity S_c occurs at the steepest slope in Fig. 2(a), being $S_c = \sqrt{\eta_{\mathrm{ext}}\eta_{\mathrm{int},c}\nu_c^2}^{-1}$. Here, ν_c is the fringe visibility, with $\eta_{\mathrm{int},c}$ denoting the mean optical transmissivity inside of the interferometer, and η_{ext} is the external system efficiency outside of the interferometer (including optical filters, fiber coupling, and nonunity detector efficiency). For the quantum scheme, the phase sensitivity at the steepest slope is $S_q = \sqrt{\eta_{\mathrm{ext}}(\eta_{\mathrm{int},q}+1)\nu_q^2}^{-1}$ (the derivation is given in the Supplemental Material [42]). Similarly to the classical sensor, $\eta_{\mathrm{int},q}$ specifies the single-photon transmissivity inside of the quantum interferometer. As both quantum and classical sensors share the same intensity-detecting scheme, their external efficiencies η_{ext} are the same. Consequently, the quantum sensor achieves an advantage over the ideal classical sensor ($\eta_{\mathrm{int},c} = 1,\ \nu_c = 1$), if

$$\sqrt{(\eta_{\mathrm{int},q}+1)\nu_q^2} > 1. \tag{3}$$

Experimentally, we measure a raw fringe visibility of $\nu_q = 0.85 \pm 0.02$, mainly limited by imperfect photonic

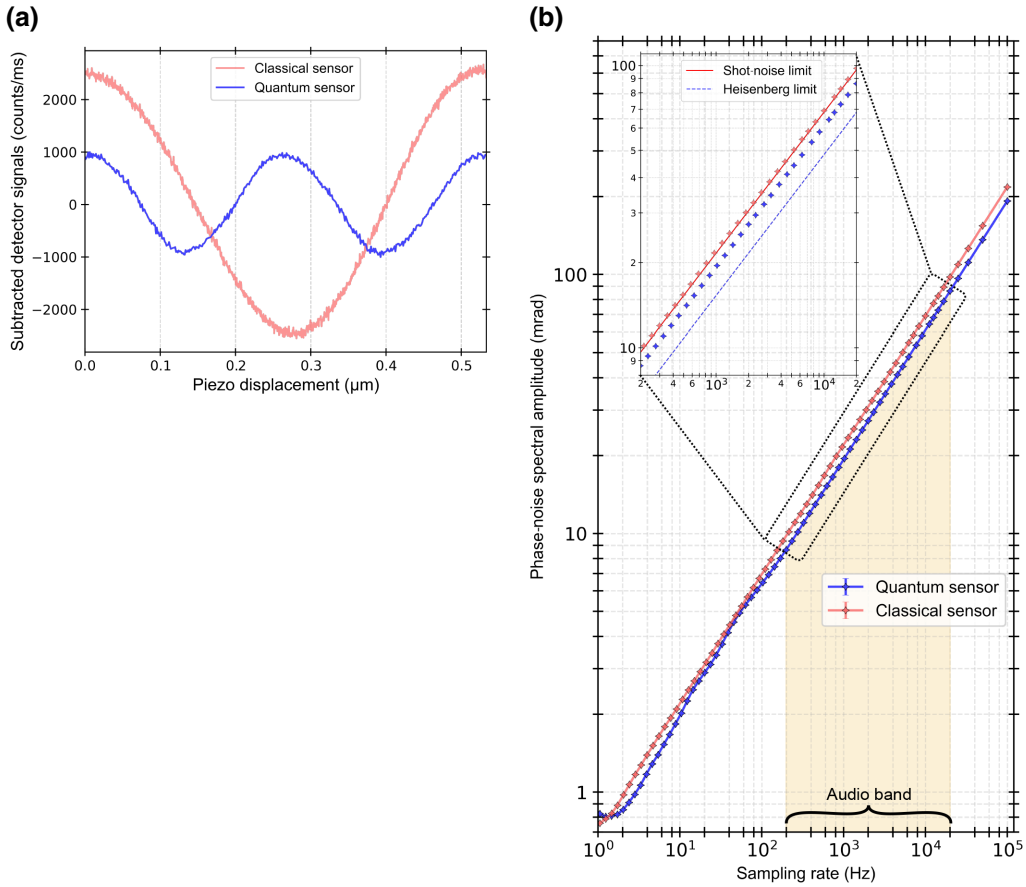

FIG. 2. Benchmarking the classical and quantum sensors. (a) The subtracted detector intensity signals $D_+ - D_-$ for the classical (red) and the quantum sensors (blue). For the same piezo displacement, the quantum sensor presents twice as many fringes, thus corroborating phase sensing with superresolution. (b) The frequency-dependent phase-noise spectral amplitudes of the classical (red) and quantum (blue) sensor. Both measurements are performed at identical photon fluxes, prior to any loss inside the interferometer. Above 200 Hz, the quantum sensor surpasses the classical sensor by a factor of 1.13 ± 0.02. In the inset, the solid and dotted lines indicate the theoretical limits of both sensors at the used photon rate of $R = 2.14 \times 10^6\ \mathrm{s}^{-1}$.

mode overlap and nonunity internal transmissivity $\eta_{\mathrm{int},q}$. In the worst case, the reduced visibility would be entirely determined by internal loss, which lower bounds $\eta_{\mathrm{int},q} \geq 0.74$ (see the Supplemental Material [42]). This results in $\sqrt{(\eta_{\mathrm{int},q}+1)\nu_q^2} \geq 1.12 > 1$, thus demonstrating a quantum sensor advantage.

To comply with the demands of sensing applications, we experimentally infer the frequency-dependent phase sensitivities S_c and S_q. To this end, we measure the spectral amplitudes of the phase noise for both the quantum and the classical sensor. As shown in Fig. 2(b), for sampling frequencies above $f = 1$ Hz, both sensors show the expected phase-noise increase with a square-root power scaling. The fit to the data shows that the classical sensor operates merely 1.5% above the fundamental SNL. Above 200 Hz, the quantum sensor surpasses the SNL by a factor of 1.13 ± 0.02, matching the predicted advantage of and S_q/S_c (as defined at the very end of the previous paragraph). Here, we note that the enhancement is sometimes defined as the square of the signal-to-variance ratio [33,43–45] but the associated enhancement factor 1.28 ± 0.04 may be confusing, as it does not directly reflect the improvement in the phase sensitivity.

A remarkable result is that our multiphoton quantum sensing scheme shows sub-shot-noise performance up to sampling rates of $f = 100$ kHz, which is at least 4 orders of magnitude higher than in previous approaches [2,15,16].

III. A QUANTUM OPTICAL MICROPHONE

The much-increased frequency bandwidth of the quantum sensor significantly broadens the range of possible applications. Capitalizing on the quantum advantage across the entire audio band of human speech (200–20000 Hz), we demonstrate the easy applicability of our sensor by implementing a quantum optical microphone, by analogy with a laser microphone [46]. Our intention is to make the quantum advantage audible, thus providing a human experience of a quantum phenomenon.

To convert acoustic waves to an optical signal, we develop an acousto-optical transducer. As shown in Fig. 3(a), we replace the SM in the interferometer by a 70-μm thin glass plate on which a small dielectric mirror is glued (mirror dimensions $2 \times 2 \times 0.5\ \mathrm{mm}^3$). We excite the membrane using a loudspeaker placed 3.5 cm behind the membrane. Single-tone frequency-response measurements show a nearly flat response across the human audio band up to 15 kHz [see Fig. 3(b)]. The membrane response linearity as a function of the speaker volume V_{A} is additionally confirmed (see the Supplemental Material [42]).

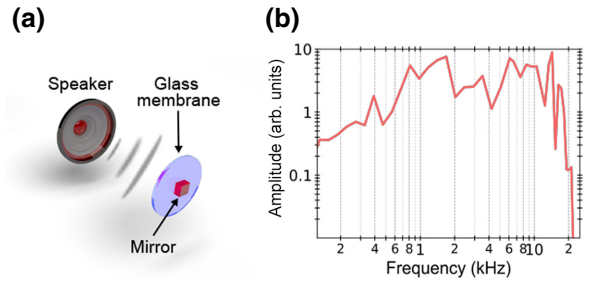

FIG. 3. The acousto-optical transducer. (a) A glass membrane with a diameter of 12.7 mm and a thickness of 70 μm translates acoustic pressure waves into a physical displacement. Photons are reflected by a small dielectric mirror that is glued on the membrane (mirror size $2 \times 2 \times 0.5$ mm^3). (b) The frequency response of the transducer under single-tone excitation.

We then use our setup to record audio snippets from a medically approved speech-recognition test [the Oldenburger sentence recognition (OLSA) test [47–49]; see the Supplemental Material [42]]. The test is based on 600 words, distributed over 120 five-word-long sentences. Words are played through the loudspeaker and recorded with the classical and quantum microphones at a sampling rate of $f = 20$ kHz. The SNR of these recordings is adjusted in 22 steps via the loudspeaker volume V_A, measured in $\mathrm{dB_{SPL}}$ (where SPL is the sound pressure level). In total, we record $2 \times 22 \times 600 = 26\,400$ words. When expressing the SNR and volume in decibels, we expect a linear relationship:

$$\mathrm{SNR}_i = \alpha_i V_A + \beta_i. \tag{4}$$

Here, the subscript $i = c, q$ denotes the classical and quantum microphone, α_i is the proportionality factor, and β_i is the SNR at $V_A = 0\ \mathrm{dB_{SPL}}$. Analysis of all audio data shows that both setups provide the same responsiveness: $\alpha_c = 0.95 \pm 0.02$, $\alpha_q = 0.95 \pm 0.02$. As expected, the baseline SNR of the quantum microphone is higher, i.e., $\beta_c = 6.20 \pm 0.22\ \mathrm{dB_{SPL}}$ and $\beta_q = 7.04 \pm 0.20\ \mathrm{dB_{SPL}}$, already indicating the quantum enhancement (see the Supplemental Material [42]).

To demonstrate that the quantum improvement is actually perceivable by humans, we subsequently conduct the medically approved speech-recognition test on $n = 45$ subjects in a calibrated sound-studio environment at the audiology department of the Olgahospital in Stuttgart (Germany). All individuals are German native speakers and normal hearing is initially verified by a pure-tone audiometry test. To infer each subject's individual speech-recognition threshold (SRT, defined as the 50% success threshold of understood words), they listen to randomized five-word sentences based on the German grammatical structure (name–verb–numeral–adjective–object). After communicating what they hear, the success percentage of understood words is noted. Repetition of this procedure at different SNRs eventually results in a psychometric function from which we obtain the minimum required volume V_A to reach the SRT. All subjects are familiarized with the test procedure by initial training on ten sentences. Then, the SRT of each subject is inferred with 2×30 sentences that are recorded using the classical and quantum microphones. Although the OLSA test is resilient against training, we eliminate potential biasing by randomizing the test order between subjects. Bias due to fatigue is avoided with a 5-min break after 30 sentences.

Figure 4(a) shows the difference of the SRT values between the quantum and classical microphones. Points below the difference SRT of 0 $\mathrm{dB_{SPL}}$ indicate improved speech-recognition performance with the quantum microphone. The data show immediately that for the vast majority of subjects (71%), the recordings with the quantum microphone lead to a reduced threshold volume; in other words, a quantum advantage is observed. In Fig. 4(b), the data are grouped into a histogram, from which we deduce a mean improvement of $-0.57\ \mathrm{dB_{SPL}}$, with a 95% confidence interval of $\pm 0.44\ \mathrm{dB_{SPL}}$. The width of the histogram (one standard deviation) is $1.45\ \mathrm{dB_{SPL}}$, which is in accordance with the systematic accuracy of single rounds of the OLSA test [47–49]. The consideration that we perform $n = 45$ measurements leads to an improvement of the relevance of our results; i.e., according to the square-root law [50], the quantum advantage is confirmed with a standard deviation of $(1.45\ \mathrm{dB_{SPL}})/\sqrt{n} = 0.22\ \mathrm{dB_{SPL}}$. Additionally, a statistical t test with the hypothesis "The quantum microphone does not result in an advantage" is rejected with a p value of $p = 0.006$, which is well below the commonly accepted threshold value of $p = 0.05$ (see the Supplemental Material [42]).

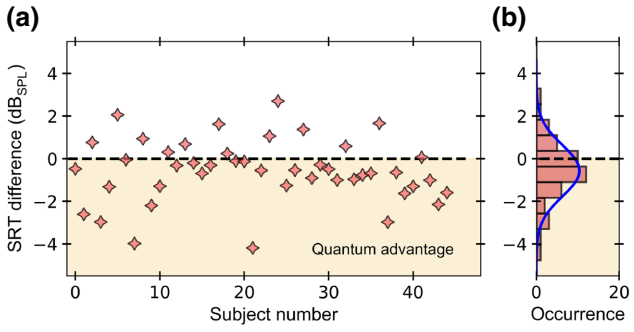

FIG. 4. The results of the speech-recognition test on $n = 45$ individuals. (a) Each individual's difference in SRT for speech snippets recorded with the classical and quantum microphone, respectively. The data below the dashed line represent a quantum improvement. (b) The histogram of all data points. The quantum microphone reduces the volume level required to achieve the SRT by $-0.57\ \mathrm{dB_{SPL}}$, with a 95% confidence interval of $\pm 0.44\ \mathrm{dB_{SPL}}$.

IV. CONCLUSIONS

We demonstrate a simple quantum-enhanced sub-shot-noise optical phase-sensing scheme with common-mode noise rejection at high sampling rates up to $f = 100$ kHz. These results are enabled by path-polarization-state quantum engineering, which allows us to measure signals with standard intensity detectors, thus overcoming the sampling-rate issue in quantum optical sensing. The possibility of using identical detection schemes in both classical and quantum sensing schemes makes it even more straightforward to perform benchmarking. As such, we demonstrate a 1.13 ± 0.02 times sensitivity improvement for the quantum sensor and further improvements are realistic using optimized low-loss optics.

To highlight the reliability and applicability of the quantum sensing scheme, we then develop a quantum optical microphone for recording human speech. By comparing classical and quantum microphones at identical photon numbers, we show that the quantum microphone records sound at a significantly reduced baseline noise level. These observations are subsequently confirmed in a medical speech-recognition test on $n = 45$ subjects, which shows that the speech-recognition threshold is improved by -0.57 $\mathrm{dB_{SPL}}$ on average, thus confirming that humans can hear the quantum advantage. We believe that the combination of quantum sensors and human experiences is likely to trigger further interest in the field.

We mention that as a quantum optical microphone, the presented application represents a specific proof-of-concept demonstration that would be outperformed by classical measurements at higher intensities or shorter wavelengths. However, a direct advantage over classical schemes could be obtained in some specific scenarios, such as applications involving biological samples, chemical reactions, or atomic spin ensembles, which are sensitive to light exposure and/or short-wavelength photons [31,51–55]. In this sense, our quantum light source already operates within the favorable second biological window, BW-II ($1000 - 1350$ nm) [56]. To show an exploitable quantum advantage, the light flux of our source would have to be increased to the level of a few hundreds of nanowatts. In that regard, a previous work has already demonstrated photon-pair beams at power levels of 0.3 μW, while still operating in the district photon-pair regime [57]. At that point, the intensity detectors need to show a superior performance in opto-electronic conversion with noise figures of merit below the photonic shot noise. As we show experimentally in the Supplemental Material [42], suitable performance can actually be achieved by several commercially available InGaAs camera modules, thus putting quantum bioimaging within realistic reach.

Additionally, we also believe that it would be interesting to study the regime beyond distinct photon-pair fluxes and use the effect of stimulated emission, similar to SU(1,1) interferometry [11,58,59]. On the one hand, higher power levels may further increase the quantum sensing enhancement factor, while on the other, path-polarization-state engineering may provide a pathway to introduce common-mode noise suppression in these schemes.

Overall, we believe that our work provides a powerful addition to the toolbox of quantum optical sensing approaches, promising enhanced variety and advances in the field.

ACKNOWLEDGMENTS

We thank Barbara Baum, Annette Zechmeister, and Frank Schreiber for their participation in designing and manufacturing the mirror membrane used for this experiment. We also thank Louis Davide, Stefan Gaget, and Markus Kleinhansl for helpful discussions regarding the statistical evaluation, Marwa Garsi and Katharina V. Wutz for counseling regarding the design of the figures and Élie Gouzien for fruitful discussions regarding the theoretical framework. We thank Andreas Vollmer for support on the measurements of the WSWP performance. We thank Lukas Niechziol for proofreading and fruitful discussions. D.M.L. acknowledges the U.S. Department of Energy, the Office of Science, under Awards No. DE-SC0019174 and No. DE-Ac02-76SF00515. S.B. acknowledges support from the Carl Zeiss Foundation, the Center for Integrated Quantum Science and Technology (IQST), the German Research Foundation (DFG), the Federal Ministry of Education and Research (BMBF, project SiSiQ, "Silicon Photonics in Secure Quantum Networks"), and the Federal Ministry for Economic Affairs and Energy (BMWi, project PlanQK, "Platform and Ecosystem for Quantum Assisted Artificial Intelligence"). F.K., J.W., and R.N. acknowledge the support of the Center for Integrated Quantum Science and Technology (IQST), the GRK 2642 program ("Towards Graduate Experts in Photonic Quantum Technologies"), the European Science Council via European Research Council (ERC) grant SMeL ("Electric Field Imaging of Single Molecular Charges by a Quantum Sensor"), and the Max Planck Society.

R.N., J.S., and T.L. performed the experiment; R.N. and F.K. analysed the data. F.K. designed the experiment and provided experimental assistance. R.N. and F.K. wrote the paper. F.K., J.W., and C.M.G. supervised the project. R.S., D.M.L., V.V., C.B., and J.V. assisted with discussions and design ideas in the development of the mirror membrane. M.T.P.Z. and R.B. provided helpful discussions about the analysis of the statistical data. C.B. provided the theoretical framework for the experiment. S.B. provided laboratory space for recording the sound files. R.B. provided the sound-studio environment to carry out the OLSA tests. R.K. and S.B. developed and provided experimental equipment. R.K. and R.N. built up the classical laser source. All authors provided helpful comments on the manuscript.

[1] I. Coddington, W. C. Swann, L. Nenadovic, and N. R. Newbury, Rapid and precise absolute distance measurements at long range, Nat. Photonics **3**, 351 (2009).

[2] V. Cimini, M. Mellini, G. Rampioni, M. Sbroscia, L. Leoni, M. Barbieri, and I. Gianani, Adaptive tracking of enzymatic reactions with quantum light, Opt. Express **27**, 35245 (2019).

[3] Y. J. Kim, P. M. Celliers, J. H. Eggert, A. Lazicki, and M. Millot, Interferometric measurements of refractive index and dispersion at high pressure, Sci. Rep. **11**, 5610 (2021).

[4] B. R. Masters, Superresolution Optical Microscopy: The Quest for Enhanced Resolution and Contrast, Springer 227, 54 (2020).

[5] M. Conroy and D. Mansfield, Measuring microscale devices, Nat. Photonics **2**, 661 (2008).

[6] V. Giovannetti, S. Lloyd, and L. MacCone, Quantum Metrology, Phys. Rev. Lett. **96**, 010401 (2006).

[7] R. Demkowicz-Dobrzański, M. Jarzyna, and J. Kołodyński, Quantum limits in optical interferometry, Prog. Opt. **60**, 345 (2015).

[8] S. Slussarenko, M. M. Weston, H. M. Chrzanowski, L. K. Shalm, V. B. Verma, S. W. Nam, and G. J. Pryde, Unconditional violation of the shot-noise limit in photonic quantum metrology, Nat. Photonics **11**, 700 (2017).

[9] C. M. Caves, Quantum-mechanical noise in an interferometer, Phys. Rev. D **23**, 1693 (1981).

[10] J. W. Pan, Z. B. Chen, C. Y. Lu, H. Weinfurter, A. Zeilinger, and M. Zukowski, Multiphoton entanglement and interferometry, Rev. Mod. Phys. **84**, 777 (2012).

[11] M. V. Chekhova and Z. Y. Ou, Nonlinear interferometers in quantum optics, Adv. Opt. Phot. **8**, 104 (2016).

[12] G. Brida, M. Genovese, and I. R. Berchera, Experimental realization of sub-shot-noise quantum imaging, Nat. Photonics **4**, 227 (2010).

[13] A. E. Ulanov, I. A. Fedorov, D. Sychev, P. Grangier, and A. I. Lvovsky, Loss-tolerant state engineering for quantum-enhanced metrology via the reverse Hong-Ou-Mandel effect, Nat. Commun. **7**, 11925 (2016).

[14] J. P. Dowling, Quantum optical metrology—The lowdown on high-N00N states, Contemp. Phys. **49**, 125 (2008).

[15] I. Afek, O. Ambar, and Y. Silberberg, High-NOON states by mixing quantum and classical light, Science **328**, 879 (2010).

[16] T. Ono, R. Okamoto, and S. Takeuchi, An entanglement-enhanced microscope, Nat. Commun. **4**, 2426 (2013).

[17] R. J. Birrittella, P. M. Alsing, and C. C. Gerry, The parity operator: Applications in quantum metrology, AVS Quantum Sci. **3**, 014701 (2021).

[18] M. Malik, M. Erhard, M. Huber, M. Krenn, R. Fickler, and A. Zeilinger, Multi-photon entanglement in high dimensions, Nat. Photonics **10**, 248 (2016).

[19] X. C. Yao, T. X. Wang, P. Xu, H. Lu, G. S. Pan, X. H. Bao, C. Z. Peng, C. Y. Lu, Y. A. Chen, and J. W. Pan, Observation of eight-photon entanglement, Nat. Photonics **6**, 225 (2012).

[20] R. H. Hadfield, Single-photon detectors for optical quantum information applications, Nat. Photonics **3**, 696 (2009).

[21] C. Kim and P. Kumar, Quadrature-Squeezed Light Detection Using a Self-Generated Matched Local Oscillator, Phys. Rev. Lett. **73**, 1605 (1994).

[22] A. Eckstein, A. Christ, P. J. Mosley, and C. Silberhorn, Highly Efficient Single-Pass Source of Pulsed Single-Mode Twin Beams of Light, Phys. Rev. Lett. **106**, 013603 (2011).

[23] R. E. Slusher, P. Grangier, A. LaPorta, B. Yurke, and M. J. Potasek, Pulsed Squeezed Light, Phys. Rev. Lett. **59**, 2566 (1987).

[24] V. Boyer, A. M. Marino, R. C. Pooser, and P. D. Lett, Entangled images from four-wave mixing, Science **321**, 544 (2008).

[25] H. Vahlbruch, M. Mehmet, K. Danzmann, and R. Schnabel, Detection of 15 dB Squeezed States of Light and their Application for the Absolute Calibration of Photoelectric Quantum Efficiency, Phys. Rev. Lett. **117**, 110801 (2016).

[26] W. E. Moerner, The photorefractive effect, Nature **371**, 476 (1994).

[27] F. Kaiser, B. Fedrici, A. Zavatta, V. D'Auria, and S. Tanzilli, A fully guided-wave squeezing experiment for fiber quantum networks, Optica **3**, 362 (2016).

[28] T. Kashiwazaki, N. Takanashi, T. Yamashima, T. Kazama, K. Enbutsu, R. Kasahara, T. Umeki, and A. Furusawa, Continuous-wave 6-dB-squeezed light with 2.5-THz-bandwidth from single-mode PPLN waveguide, APL Photonics **5**, 036104 (2020).

[29] U. L. Andersen, T. Gehring, C. Marquardt, and G. Leuchs, 30 years of squeezed light generation, Phys. Scr. **91**, 053001 (2016).

[30] R. Schnabel, Squeezed states of light and their applications in laser interferometers, Phys. Rep. **684**, 1 (2017).

[31] F. Wolfgramm, A. Cerè, F. A. Beduini, A. Predojević, M. Koschorreck, and M. W. Mitchell, Squeezed-Light Optical Magnetometry, Phys. Rev. Lett. **105**, 053601 (2010).

[32] R. Demkowicz-Dobrzański, J. Kołodyński, and M. Guţa, The elusive Heisenberg limit in quantum-enhanced metrology, Nat. Commun. **3**, 1063 (2012).

[33] F. Hudelist, J. Kong, C. Liu, J. Jing, Z. Y. Ou, and W. Zhang, Quantum metrology with parametric amplifier-based photon correlation interferometers, Nat. Commun. **5**, 3049 (2014).

[34] S. S. Szigeti, R. J. Lewis-Swan, and S. A. Haine, Pumped-Up SU(1,1) Interferometry, Phys. Rev. Lett. **118**, 150401 (2017).

[35] X. Y. Zou, L. J. Wang, and L. Mandel, Induced Coherence and Indistinguishability in Optical Interference, Phys. Rev. Lett. **67**, 318 (1991).

[36] L. J. Wang, X. Y. Zou, and L. Mandel, Induced coherence without induced emission, Phys. Rev. A **44**, 4614 (1991).

[37] T. J. Herzog, J. G. Rarity, H. Weinfurter, and A. Zeilinger, Frustrated Two-Photon Creation via Interference, Phys. Rev. Lett. **72**, 629 (1994).

[38] G. B. Lemos, V. Borish, G. D. Cole, S. Ramelow, R. Lapkiewicz, and A. Zeilinger, Quantum imaging with undetected photons, Nature **512**, 409 (2014).

[39] G. J. Machado, G. Frascella, J. P. Torres, and M. V. Chekhova, Optical coherence tomography with a nonlinear interferometer in the high parametric gain regime, Appl. Phys. Lett. **117**, 094002 (2020).

[40] I. Kviatkovsky, H. M. Chrzanowski, E. G. Avery, H. Bartolomaeus, and S. Ramelow, Video-rate imaging with

undetected photons, Laser Photonics Rev. **15**, 2000327 (2021).
[41] P. Vergyris, C. Babin, R. Nold, E. Gouzien, H. Herrmann, C. Silberhorn, O. Alibart, S. Tanzilli, and F. Kaiser, Two-photon phase-sensing with single-photon detection, App. Phys. Lett. **117**, 024001 (2020).
[42] See the Supplemental Material at http://link.aps.org/supplemental/10.1103/PRXQuantum.3.020358 for providing further details on theoretical calculations, experimental benchmarking, as well as characterization of experimental equipment.
[43] W. Du, J. F. Chen, Z. Y. Ou, and W. Zhang, Quantum dense metrology by an SU(2)-in-SU(1,1) nested interferometer, Appl. Phys. Lett. **117**, 024003 (2020).
[44] G. Frascella, E. E. Mikhailov, N. Takanashi, R. V. Zakharov, O. V. Tikhonova, and M. V. Chekhova, Wide-field SU(1,1) interferometer, Optica **6**, 1233 (2019).
[45] M. Fox, Quantum Optics: An Introduction, Oxford University Press, Oxford 15, 143 (2006).
[46] J. T. Veligdan, Laser Microphone, U.S. Patent No. US6147787A (2000).
[47] K. C. Wagener, V. Kuhnel, B. Kollmeier, T. Brand, and B. Kollmeier, Entwicklung und Evaluation eines Satztests für die deutsche Sprache I: Design des Oldenburger Satztests, Z Audiol. **38**, 1 (1999).
[48] K. C. Wagener, V. Kuhnel, B. Kollmeier, T. Brand, and B. Kollmeier, Entwicklung und Evaluation eines Satztests für die deutsche Sprache Teil II: Optimierung des Oldenburger Satztests, Z Audiol. **38**, 44 (1999).
[49] K. Wagener, T. Brand, and B. Kollmeier, Entwicklung und Evaluation eines Satztests für die deutsche Sprache Teil III: Optimierung des Oldenburger Satztests, Z Audiol. **38**, 86 (1999).
[50] D. Freedman, An empirical form of the square root law and the central limit theorem, Math. Proc. Camb. Philos. Soc. **80**, 287 (1976).
[51] V. Cimini, I. Gianani, L. Ruggiero, T. Gasperi, M. Sbroscia, E. Roccia, D. Tofani, F. Bruni, M. A. Ricci, and M. Barbieri, Quantum sensing for dynamical tracking of chemical processes, Phys. Rev. A **99**, 053817 (2019).
[52] Y. Fu, H. Wang, R. Shi, and J. Cheng, Characterization of photodamage in coherent anti-Stokes Raman scattering microscopy, Opt. Express **14**, 3942 (2006).
[53] B. Li, C. Wu, M. Wang, K. Charan, and C. Xu, An adaptive excitation source for high-speed multiphoton microscopy, Nat. Methods **17**, 163 (2020).
[54] L. Schermelleh, A. Ferrand, T. Huser, C. Eggeling, M. Sauer, O. Biehlmaier, and G. P. C. Drummen, Super-resolution microscopy demystified, Nat. Cell Biol. **21**, 72 (2019).
[55] S. Wäldchen, J. Lehmann, T. Klein, S. van de Linde, and M. Sauer, Light-induced cell damage in live-cell super-resolution microscopy, Sci. Rep. **5**, 15348 (2015).
[56] B. del Rosal, I. Villa, D. Jaque, and F. Sanz-Rodríguez, *In vivo* autofluorescence in the biological windows: The role of pigmentation, J. Biophoton **9**, 1059 (2016).
[57] B. Dayan, A. Pe'er, A. A. Friesem, and Y. Silberberg, Nonlinear Interactions with an Ultrahigh Flux of Broadband Entangled Photons, Phys. Rev. Lett. **94**, 043602 (2005).
[58] B. Yurke, S. L. Mccall, and J. R. Klauder, SU(2) and SU(1,1) interferometers, Phys. Rev. A **33**, 4033 (1986).
[59] Z. Y. Ou and X. Li, Quantum SU(1,1) interferometers: Basic principles and applications, APL Photonics **5**, 080902 (2020).